Journal of Photochemistry & Photobiology, A: Chemistry 443 (2023) 114838

Contents lists available at ScienceDirect

Journal of Photochemistry & Photobiology, A: Chemistry

journal homepage: www.elsevier.com/locate/jphotochem

Green synthesis of photocatalytic TiO_2/Ag nanoparticles for an efficient water remediation

Maria Cantarella [a], Marco Mangano [a], Massimo Zimbone [a], Gianfranco Sfuncia [b], Giuseppe Nicotra [b], Elena Maria Scalisi [c], Maria Violetta Brundo [c], Anna Lucia Pellegrino [d], Federico Giuffrida [a,e], Vittorio Privitera [b], Giuliana Impellizzeri [a,*]

[a] CNR-IMM, Via S. Sofia 64, 95123 Catania, Italy
[b] CNR-IMM, Z.I. VIII Strada 5, 95121 Catania, Italy
[c] Department of Biological, Geological and Environmental Science, University of Catania, Via Androne 81, 95124 Catania, Italy
[d] Department of Chemical Science, University of Catania, INSTM UdR Catania, Viale Andrea Doria 6, 95125 Catania, Italy
[e] Department of Physics and Astronomy, University of Catania, Via Santa Sofia 64, 95123 Catania, Italy

ARTICLE INFO

Keywords:
Titania
Silver
Green methods
Photocatalysis
Water treatment

ABSTRACT

This work reports a green method to produce efficient photocatalytic nanopowders. Titanium dioxide nanoparticles were easily synthetized by an extract of Thymus vulgaris, and then decorated with commercial silver nanoparticles. A detailed morphological, structural, and chemical characterization was performed by scanning electron microscopy (SEM), Brunauer-Emmett-Teller (BET) adsorption–desorption of N_2, Fourier transform infrared spectroscopy (FTIR), X-ray diffraction analysis (XRD), Raman spectroscopy, transmission electron microscopy (TEM), and UV–Vis spectroscopy. The synthetized TiO_2 nanoparticles showed a mean size of 10–15 nm, and had the anatase crystallographic phase. The photocatalytic efficiency of the TiO_2 nanoparticles was demonstrated by the photo-degradation under UV-light irradiation of different pollutants in aqueous solution (methylene blue, diclofenac, and sodium dodecyl sulfate). TiO_2 was coupled to Ag nanoparticles with different percentage in weight (from 0.25 to 3%), to investigate an eventual improvement of its photocatalytic efficiency. The best photocatalytic composite among the tested compositions was the one with the lowest Ag percentage (0.25%). Zebrafish embryo toxicity tests ruled out the toxicity of the synthetized nanoparticles. The present results offer a new, green, and easy method to prepare TiO_2/Ag nanoparticles with high photocatalytic efficiency. The proposed materials are therefore promising for applications in photocatalysis, especially for wastewater remediation and reuse.

1. Introduction

Titanium dioxide (TiO_2), usually called *titania*, is a semiconducting metal oxide that has received a great attention since the discovery of the photocatalytic water splitting on a TiO_2 electrode under ultraviolet (UV) light in 1972 [1]. Since then, the scientific community has reserved huge efforts to the research of this material [2–8]. The interest in TiO_2 is mainly given by its low cost, inert nature, and photocatalytic aptitude, which make it attractive for applications in many areas, ranging from environment [9] to energy [1]. In the last 10 years, our group has dealt with nanostructured TiO_2 as efficient photocatalyst for wastewater treatment [10–23].

Looking for new methods for an effective removal of contaminants from water is currently a real challenge. Due to the population growth, the freshwater resources are less available and for this reason, the use of reclaimed water, for example for irrigation, could be a valid solution to reduce the problem of water scarcity. The main problem associated with the reclaimed water is the presence of many contaminants that the traditional water treatment methods are not able to effectively remove. Examples of these pollutants are: polycyclic aromatic hydrocarbons,

* Corresponding author.
E-mail addresses: maria.cantarella@ct.infn.it (M. Cantarella), marco.mangano@dfa.unict.it (M. Mangano), massimo.zimbone@ct.infn.it (M. Zimbone), gianfranco.sfuncia@imm.cnr.it (G. Sfuncia), giuseppe.nicotra@cnr.it (G. Nicotra), elenamaria.scalisi@unict.it (E. Maria Scalisi), mvbrundo@unict.it (M. Violetta Brundo), annalucia.pellegrino@unict.it (A. Lucia Pellegrino), federico.giuffrida@dfa.unict.it (F. Giuffrida), vittorio.privitera@imm.cnr.it (V. Privitera), giuliana.impellizzeri@ct.infn.it (G. Impellizzeri).

https://doi.org/10.1016/j.jphotochem.2023.114838
Received 16 December 2022; Received in revised form 8 May 2023; Accepted 9 May 2023
Available online 11 May 2023

produced by incomplete combustion of coal, gas, wood, and oil, and categorized as probably carcinogenic to humans; pharmaceutical and personal care products that have potential adverse ecotoxicological impacts or human health risks if released into environment; pesticides that are toxic for humans and other organisms; phthalate esters, used as plastic additives, could affect ecological conditions of water systems [24].

Nowadays, TiO_2 in the form of nanoparticles is the titania most commercially available and mainly employed in real photocatalytic applications [4].

Many methods are traditionally used for the preparation of TiO_2 nanoparticles, such as sol–gel synthesis [25], chemical reduction [26], thermal decomposition [27], photochemical reduction [28], electrochemical synthesis [29], hydrothermal method [30], laser irradiation [14], and pyrolysis [31]. However, these methods often require harsh and energy-demanding synthesis conditions and they also involve the use of toxic or hazardous chemicals, such as the traditional corrosive and flammable reducing agents [32]. For all these reasons their application in a large scale will be limited in the future, and there is a growing need to develop new synthesis processes: economic and environmental-friendly. Therefore, the syntheses of TiO_2 nanoparticles by green approaches, namely using microorganisms or plant extracts, are receiving enormous attention [33,34]. In particular, plant extracts contain numerous water soluble phytoconstituents (e.g. polyphenols, flavonoids, terpenoids, quinones, catechins, amine, etc.) that act as stabilizing agents during the formation of TiO_2 nanoparticles [35–37].

The Thymus vulgaris is a plant native in the Mediterranean regions, and it is widespread in Sicily (Italy). This perennial semi-evergreen bush is used as an aromatic plant to flavor foods and liqueurs, and as a medicinal plant for its antimicrobial and antioxidative properties to treat various diseases such as bronchitis and gastrointestinal disorders [38–40]. The Thymus vulgaris is also employed in cosmetics to prepare products for hair and skin care [38,40].

In this work we reported an experimental study on a green synthesis of TiO_2 nanoparticles in the anatase phase, by the original use of the Thymus vulgaris, for application in wastewater treatment. The addition of Ag nanoparticles helped in improving the photocatalytic efficiency of the titania thanks to the electron-scavenger behavior of the noble metals [3–5,8,11]. Peculiar attention was devoted to the eventual toxicity of the synthetized nanopowders.

2. Experimental

2.1. Preparation methods

Commercial TiO_2 nanoparticles (mixture of rutile and anatase crystalline phases, <100 nm particle size, 99.5% purity) were purchased from Merck (Darmstadt, Germany) and used as reference material.

TiO_2 powders were synthetized via a thyme extract [36,37]. A plant of Thymus vulgaris was purchased from a local Sicilian market. The leaves were collected and washed with deionized water to remove dust and potential contaminations; then they were dried for two days at room temperature. The dried leaves were crushed with an agate mortar so to obtain fine powders; ~5 g of these powders were boiled in ~30 mL of deionized water for 10 min. The obtained mixture was filtered and the green extract was collected in a vial and kept at 4 °C for successive use. Titanium tetra-isopropoxide ($C_{12}H_{28}O_4Ti$), used as Ti precursor, was purchased from Merck (99.999% of purity) and used as received. A quantity of 6 mL of this precursor were mixed with 5 mL of thyme extract and 50 mL of deionized water. The mixture was stirred on a hot plate equipped with a reflux condenser for 4 h at 50 °C. The obtained precipitate was separated from the solution by centrifugation at 6000 rpm for 15 min. The precipitate, orange in color, was washed with deionized water and then dried at 80 °C overnight. Finally, the powders were annealed at 500 °C for 3 h, becoming white.

A quantity of 0.1 g of the as-prepared TiO_2 powders were mixed in an agate mortar with different amount of commercial Ag nanoparticles (<100 nm particle size, 99.5% purity, purchased from Merck). In order to obtain a homogeneous blending of the two types of powders, few mL of water/ethanol (with a ratio 50/50) were added during the mixing procedure. Then the mixture was dried at 70 °C for a couple of hours and after annealed at 450 °C for 3 h. Five different composites, with five different percentage of Ag nanoparticles (from 0.25 to 3% in weight respect to the TiO_2), were prepared with this procedure: TiO_2 + Ag 0.25%, TiO_2 + Ag 0.5%, TiO_2 + Ag 1%, TiO_2 + Ag 2%, TiO_2 + Ag 3%.

2.2. Characterizations

The morphology of the synthetized powders was investigated by scanning electron microscopy (SEM), with a field emission Zeiss Supra 25 microscope (Jena, Germany), operating at 5 kV.

The textural properties of the materials were determined by Brunauer-Emmett-Teller (BET) adsorption–desorption of N_2 at −196 °C using a Micromeritics Tristar II Plus 3020 (Norcross, Georgia, United States), after a pre-treatment of out-gassing at 100 °C overnight.

Fourier transform infrared spectra (FTIR) were obtained by a JASCO FT/IR-4700 (Tokyo, Japan) spectrometer (accuracy: ± 0.01 cm^{-1}, resolution: 4 cm^{-1}). The samples were investigated in the form of tables, obtained by mixing the studied powders (1 mg) with KBr powders (300 mg) in an agate mortar and pressing with a press.

The structural characterization was performed by X-ray diffraction analyses (XRD), using a Smartlab Rigaku (Tokyo, Japan) diffractometer in locked coupled mode operating at 45 kV and 200 mA, equipped with a rotating anode of Cu K_α radiation. The patterns were recorded in the range 20-60° using a step of 0.02°.

Raman spectra were collected using an HR800 integrated system of Horiba Jobin Yvon (Kyoto, Japan) working in back-scattering configuration. A HeNe laser (632.8 nm) was employed as excitation source. Coaxial optics with a dichroic mirror for 633 nm light were used, and the laser light was focused via a × 100 objective onto the samples.

Transmission electron microscopy (TEM) analyses were performed using a JEOL ARM200F (Tokyo, Japan) microscope equipped with a cold field emission gun, a CESCOR spherical aberration corrector, a Centurio energy dispersive X-ray spectroscopy (EDS) detector, a Gatan Rio CMOS camera, a Gatan imaging filter (GIF) quantumER, and a Gatan K2 Summit direct detection camera for counting electron energy loss spectroscopy (EELS). TEM micrographs were acquired in conventional mode (C-TEM), with parallel beam using the Rio CMOS camera, and with convergent beam in scanning mode (S-TEM) using a Gatan High Angle Annular Dark Field (HAADF) detector. S-TEM Spectrum Imaging (SI) technique was used to collect spatially-resolved EDS and EELS data. The samples were deposited as dry powders on copper TEM grids having an ultrathin (<3 nm-thick) carbon film, supported by a lacey carbon film.

The optical characterization was obtained by measuring the diffuse reflectance spectra of the powders in the 300–800 nm wavelength range, by using a spectrophotometer Perkin-Elmer Lambda 35 (Waltham, Massachusetts, United States) equipped with an integrating sphere (RSA-PE-20, Perkin-Elmer). The band-gap energies of the synthesized materials were estimate by using the Kubelka-Munk approach and the Tauc plot as reported in Ref. [41].

2.3. Photocatalytic tests

The photocatalytic aptitude of the investigated powders was tested by different kinds of water contaminants. The first tests were performed with the methylene blue (MB) dye, a chemical compound commonly used to evaluate the photocatalytic efficiency of materials under UV-light irradiation, as indicated in the ISO 10678:2010 international standard. Before any measurement, the powders were irradiated by an UV lamp for 60 min in order to remove the hydrocarbons from the sample surfaces [42]. Thereafter, 6 mg of powders were immersed in 12

mL of aqueous solution of MB, with a starting concentration of 1.5×10^{-5} M. Before switching on the light, control experiments were conducted by keeping the solution with the powders in the dark, so to evaluate the adsorption of the MB on the beaker surface and on the sample surface. Once the saturation was reached, the MB solution containing the TiO_2 powders was irradiated by an UWAVE LED UV lamp system (Villebon-sur-Yvette, France), with an emission centered at 365 nm (full width at half maximum, FWHM, of 10 nm) and an irradiance of 10 mW/cm^2. The irradiated solution was measured at regular time intervals, with an UV–Vis spectrophotometer (Lambda 45, Perkin-Elmer; Waltham, Massachusetts, United States) in a wavelength range of 500–800 nm. The degradation of the MB was evaluated by the absorbance peak at 664 nm in the Lambert-Beer regime [43]. The decomposition of the MB dye in the absence of any photocatalysts was checked as reference.

The powders were also tested for the degradation of diclofenac, one of the most diffused nonsteroidal anti-inflammatory drug worldwide, now considered an emerging contaminant of water. The photocatalytic tests were performed with the same methodology reported above for the MB. An initial concentration of 5.5×10^{-5} M of diclofenac was used so to maximize the absorbance peak at 276 nm.

A final photocatalytic test was performed with sodium dodecyl sulfate (SDS), an anionic surfactant used in many cleaning and hygiene products for its detergent properties. Consequently, SDS is one of the main contaminant of greywater. The degradation of SDS was checked after 4 h of UV-light irradiation using a visible spectrophotometer (Hach DR 3900; Loveland, Colorado, United States) and LCK 432 cuvette kits. The starting concentration of SDS was set at 1.5×10^{-5} M.

The experimental error of the photocatalytic measurements was 5%.

2.4. Ecotoxicology tests

The eventual toxicity of the synthesized materials was evaluated on fertilized *Danio rerio* (commonly called zebrafish) eggs, according to TG 236 of OECD (2013). Fertilized eggs were collected by spawning groups at Fish Pathology and Experimental Centre of Sicily (CISS) of the Department of Veterinary Science (University of Messina). Test solutions of 0.001 g/ml for different typology of TiO_2 were prepared, dispersing the mass of 1 mg in 100 mL of osmosis water (270 μS conductivity, 26–28 °C, 6.9–7.5 pH, 6.00 ppm oxygen concentration), that is optimal for the housing of zebrafish according to Ref. [44]. Four cycles of 10 min of sonication were carried, with 3 min of break, using an ultrasonic bath (FALC Labsonic LBS2) with a frequency of 40 kHz under extractor fan, in order to disrupt any possible aggregates of nanoparticles [45]. The eggs at the blastula stage were used to the test, while the infertile eggs were discarded. As suggested by the protocol procedure, the eggs were distributed over 24-well plates with one embryo per well in order to have 20 embryos exposed to test concentration and 4 embryos in dilution water as internal plate control. Multi-well plates were set up for each titania typology, in addition multi-well plates of positive controls and negative controls were made. In the positive controls, embryos were exposed to 3,4-dichloroaniline (DCA) at the concentration of 4 mg/L in water, whereas for the negative controls embryos were exposed to water dilution [46]. Three replicates were performed for each multi-wells plates prepared. Every 24 h until 96 hpf (hours post fertilization) the acute toxicological endpoints (coagulated embryos, lack of somite formation, non-detachment of the tail, and lack of heartbeat) were assessed and quantified as observed or not observed, to determine the toxicity of the tested solutions.

3. Results and discussions

The first part of the work was dedicated to the green synthesis of TiO_2 nanoparticles by using a Thymus vulgaris extract (this material will be simply called "TiO_2" hereafter). Scientific papers on Thymus vulgaris [38–40], and on the syntheses of ZnO nanoparticles by Thymus vulgaris leaf extract [47,48] helped us in understanding the formation process of the TiO_2 nanoparticles in this work. Phytochemical analyses of Thymus vulgaris leaf extract revealed the presence phenols, flavonoids, saponins, tannins, terpenoids, and volatile oils [38,39,48]. These organic molecules acted as stabilizing agents during the synthesis of the TiO_2 nanoparticles, promoting the formation of small nanoparticles (average size of about 50 nm in Refs. [47,48]. After the synthesis, the thermal treatment at 500 °C was necessary to obtain the TiO_2 in a crystalline form, but also to remove the residual organic molecules adsorbed on the surface of the TiO_2 nanoparticles.

The TiO_2 nanoparticles obtained by the Thymus vulgaris leaf extract were deeply characterized and compared to commercial TiO_2 nanoparticles (purchased from Merck).

Fig. 1 reports two SEM images of TiO_2 synthetized with the thyme extract (a) and commercial TiO_2 nanoparticles (b). Both materials were in the form of powders. The green synthesis method led to the formation of nanoparticles with an irregular shapes and a broad size distribution, indeed the size of the nanoparticles ranged from ~10 to ~100 nm (Fig. 1 (a)). The commercial nanoparticles showed a more regular shape (mainly spherical) and size distribution (~40–50 nm) (Fig. 1 (b)). Both TiO_2 materials, and especially the TiO_2 obtained with the thyme extract, appeared stuck together as agglomerates, hindering an accurate determination of their size by the scanning electron microscopy.

The textural properties of the TiO_2 synthetized with the thyme extract were deduced by the measurements of adsorption–desorption of N_2 and application of the BET theory. The evaluations were compared with the ones of commercial TiO_2. The BET surface area (S_{BET}), the pore diameter (d_p), and the pore volume (V_p) are reported in Table 1 for the synthetized TiO_2 nanoparticles and commercial TiO_2 nanoparticles. The exposed surface area of the titania synthetized with the thyme extract

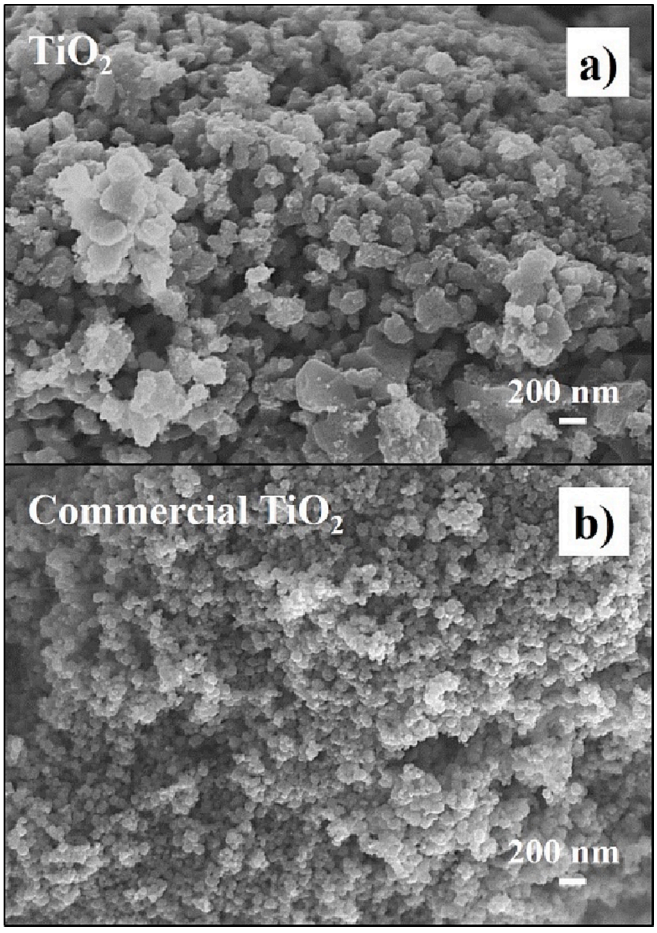

Fig. 1. SEM images of TiO_2 nanoparticles synthetized with the thyme extract (a), and commercial TiO_2 (b).

Table 1
BET surface area (S_{BET}), mean pore diameter (d_p), and pore volume (V_p) of TiO_2 and commercial TiO_2.

Catalyst	S_{BET} ($m^2\ g^{-1}$)	d_p (nm)	V_p ($cm^3\ g^{-1}$)
TiO_2	92 ± 2	10.3 ± 0.5	0.28 ± 0.02
Commercial TiO_2	68 ± 1	15.4 ± 0.8	0.32 ± 0.02

was found to be 92 m^2/g, slightly higher than the one of commercial titania (68 m^2/g). Consequently, the pore diameter and volume are lower in the synthetized TiO_2 in comparison to commercial TiO_2. In the Supplementary material the reader can also find the N_2 adsorption–desorption curves of the two TiO_2 powders (Fig. S1 (a)); the isotherms showed hysteresis loops typical of mesoporous materials [49]. Figure S1 (b) depicts the corresponding Barrett, Joyner and Halenda (BJH) pore size distributions of the two different TiO_2 powders.

FTIR spectra of the TiO_2 synthetized with the green method and commercial TiO_2 are reported in Fig. S2. Both spectra showed similar features. The broad band from ~400 to ~900 cm^{-1} is due to the titania, indeed it is correlated to the Ti-O-Ti stretching vibrations; the band at ~1630 cm^{-1} is due to the physical adsorbed water, since it is related to the H-O-H bending vibrations; while, the broad band at ~3300 cm^{-1} can be associated to the O-H stretching vibrations of the hydroxyl groups [50].

The structural characterization through XRD analyses was conducted in order to study the TiO_2 nanoparticle crystalline phase. Fig. 2 reports the patterns of TiO_2 synthetized with the thyme extract and the patterns of commercial TiO_2 nanopowders. Commercial TiO_2 showed well-defined peaks at 2θ = 25.4°, 37.9°, 48.0°, 54.1°, and 55.1° associated with 101, 004, 200, 105, and 211 reflections typical of the anatase phase (in accordance with the ICDD no.00–084-1286), but also a peak at 2θ = 27.4° characteristic of the rutile phase. This confirmed the mixture of anatase and rutile of the used commercial titania, as declared by Merck. On the other hand, the TiO_2 synthetized with the thyme extract only showed the characteristic peaks of the anatase, in accordance with the thermal treatment at 500 °C (see the Experimental section) [51]. The crystal size was estimated through the Scherrer equation [52]: $D = \frac{K\lambda}{\beta cos\theta}$, where k is a shape factor that depends on crystallite apparent radius and is equal to 0.9, λ is the X-ray wavelength, β is related to the FWHM of the peak at the angle 2θ. The D values were calculated for each sample considering an average of the values obtained for the peaks at 25.4° and 48.0°. The crystal dimensions resulted 120 ± 12 nm for the commercial TiO_2, 90 ± 9 nm for the TiO_2 synthetized with the thyme extract.

Raman spectra of the TiO_2 synthetized with the thyme extract and commercial TiO_2 nanopowders are shown in Fig. 3. The observed peaks were assigned to the two most abundant TiO_2 phases: anatase and rutile. The anatase can be recognized by three peaks at: 399, 518, and 640 cm^{-1} assigned to B_{1g}, B_{1g} + A_{1g}, and E_g vibrations, respectively, while the rutile phase is recognized by two vibrations at 448 cm^{-1} (E_g), and at 612 cm^{-1} (A_{1g}) [53]. The samples synthesized in presence of thyme showed only the peaks related to the anatase phase, in agreement with the thermal treatment at 500 °C (see the Experimental section) [51]. Thus, the Raman results confirmed the XRD analyses (the reader can refer to Fig. 2). On the other hand, the spectrum of commercial TiO_2 exhibited both the anatase and rutile features, as reported in the product card provided by Merck.

Fig. 4 reports C-TEM micrographs, EELS and EDS spectra (Fig. 4 (a), (b), and (c), respectively) for TiO_2 nanoparticles synthetized with the thyme extract. C-TEM micrographs (Fig. 4 (a) is one of them) showed aggregated TiO_2 nanoparticles, most of them with a polyhedron shape, having an average size of about 10–15 nm. Inset of Fig. 4 (a) shows a high-resolution image of a single TiO_2 nanoparticle, in which the (1 0 1) atomic planes are highlighted. The relative interplanar distance of 0.35 nm is typical of anatase TiO_2. An EELS spectrum, reported in Fig. 4 (b), shows Ti L edge, rising at about 455 eV. This edge presents two features, L_3 and L_2, respectively due to the excitation of $2p_{3/2}$ and $2p_{1/2}$ titanium core electrons. Both L_3 and L_2 features are split: the resulting fine structure is specific of the TiO_2 anatase polymorph, as reported in our previous study [23]. Inset of Fig. 4 (b) shows a TiO_2 EELS spectrum with the aforementioned titanium L edge and the oxygen K edges at 532 eV. EDS analyses, acquired in C-TEM and reported in Fig. 4 (c), showed titanium Kα and Kβ peaks, respectively at 4.51 and 4.93 keV, and oxygen Kα peak at 0.52 keV. Copper Lα, Kα and Kβ peaks, respectively at 0.93, 8.05 and 8.95 keV, and carbon Kα peak, at 0.28 keV, originated from the TEM grid. Inset of Fig. 4 (c) is an enlargement of the EDS spectrum in the 2.5–3.5 keV energy range, showing the presence of titanium Kα and Kβ escape peaks, respectively at 2.77 and 3.21 keV. Titanium K escape peaks occur when titanium K photons excite K-shell electrons in detector's silicon atoms, which can relax emitting Si Kα photons at 1.74 keV. Whenever these photons escape from the detector, spurious peaks appear in the EDS spectrum at energy equal to the difference between the analyte peak (Ti Kα or Ti Kβ) energy and silicon Kα peak energy.

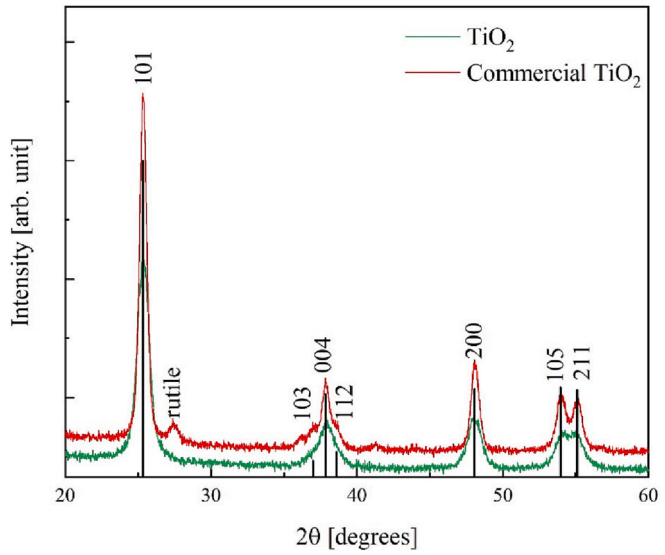

Fig. 2. XRD patterns of TiO_2 (green line), and commercial TiO_2 (red line) nanoparticles. The peak of the rutile and the peaks of the anatase are explicitly indicated.

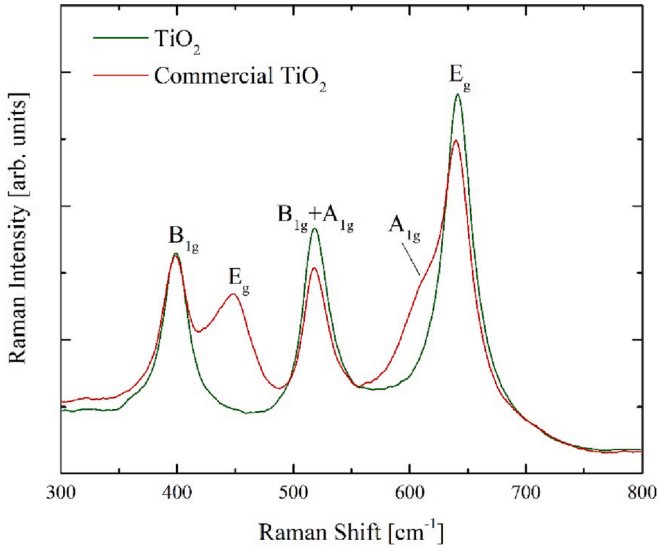

Fig. 3. Raman spectra of TiO_2 (green line), and commercial TiO_2 (red line) nanoparticles. The modes of the anatase and rutile phase are explicitly indicated.

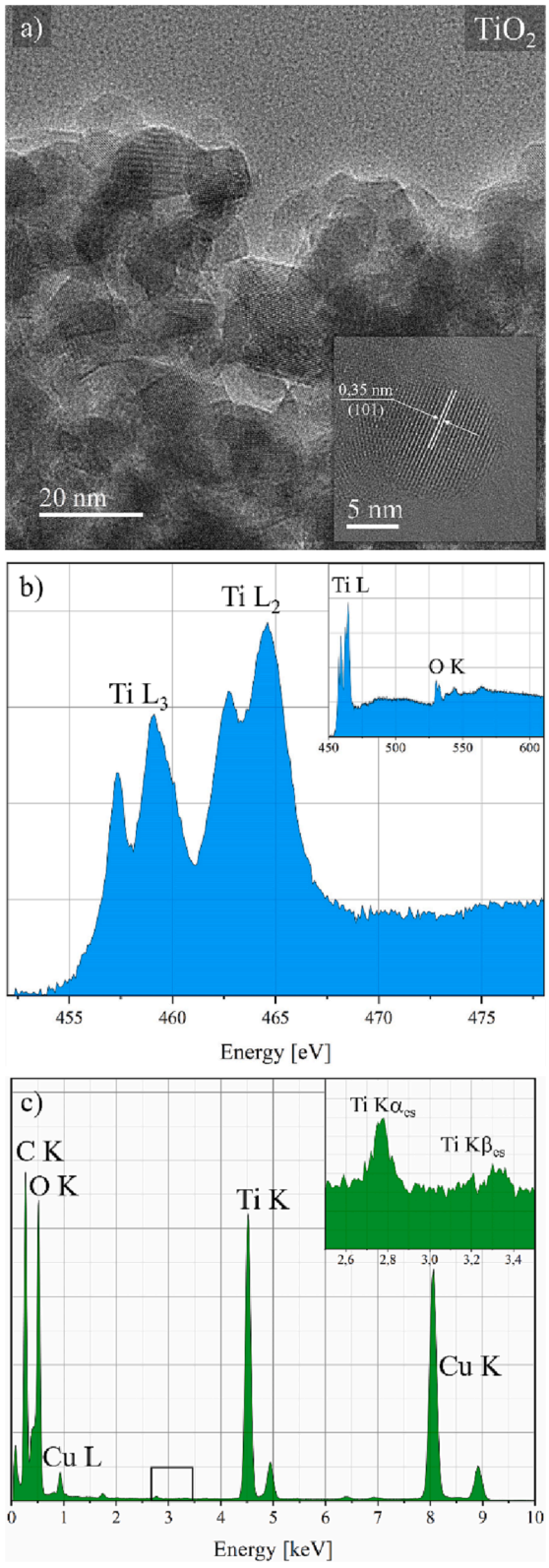

Fig. 4. (a) Conventional-TEM micrograph of TiO_2 nanoparticles, with inset showing a high-resolution image of a single nanoparticle with (101) lattice fringes; (b) EELS spectrum of Ti L edge in TiO_2 nanoparticles, with inset showing TiO_2 EELS spectrum with characteristic titanium and oxygen edges; (c) EDS spectrum for TiO_2 nanoparticles with inset showing an enlargement in the 2.5–3.5 keV energy range, evidencing the presence of titanium Kα and Kβ escape peaks.

Fig. 4 (c) also reports a low-intensity potassium Kα peak at 3.31 keV, probably coming from the thyme extract. The synthesis with the thyme produced overall pure anatase TiO_2 nanoparticles.

Fig. 5 (a) shows the diffuse reflectance spectra of TiO_2 synthetized with the thyme extract and commercial TiO_2 powders. A weak decrease of the reflectance for wavelengths higher than 450 nm is apparent, and can be related to scattering phenomena. On the other hand, the abrupt increase of the reflectivity between ~350 and ~450 nm is due to the TiO_2 adsorption edge. A blue shift of the absorption edge was observed in the TiO_2 samples presented in this work, indicating already a slightly higher band-gap energy than the one of the commercial powders. The band-gap energies of the investigated nanopowders were estimated by using the Kubelka-Munk approach and the Tauc plot as reported in Ref. [41]. Fig. 5 (b) shows $(F(R)h\nu)^{1/2}$ as a function of the photon energy $h\nu$, where $F(R)$ is the Kubelka-Munk function: $F(R) = \frac{(1-R)^2}{2R}$ (being R the reflectance). In the region above 3 eV, the curves show a linear increase with the energy. The x-axis intersections of the linear fits allowed the estimations of the band-gap energies: 3.23 ± 0.05 eV and 3.02 ± 0.05 eV for TiO_2 and commercial TiO_2, respectively. The estimated variation in the band-gap energy is surely related to the different phases of the two measured materials. Indeed, the TiO_2 nanopowders synthetized with the thyme extract are in the anatase phase (see Figs. 2, 3, and 4), having notoriously band-gap of about 3.2 eV [2]. On the other hand, commercial TiO_2 powders have a mixed phases (rutile and anatase, as declared by Merck and demonstrated by the XRD pattern reported in Fig. 2 and the Raman spectrum reported in Fig. 3), having the typical band-gap of rutile of about 3.0 eV [2].

Fig. 6 reports the photocatalytic degradation of the MB dye by means of the nanoparticles under investigations. The graph displays C/C_0 as a function of the irradiation time t, where C is the concentration of the MB after UV-light irradiation for time t, C_0 is the starting concentration of the dye. The control experiment led in the dark did not revealed any important contribution of the adsorption process. Once switched on the UV light, no degradation was observed in the case of the aqueous solution containing only MB, as expected. On the other hand, almost all the dye was degraded in only 2 h thanks to the titania synthetized with the thyme extract. A comparison with the commercial TiO_2 showed a remarkable response of the synthetized titania. In order to compare the photocatalytic activity of the two different nanopowders typologies, we applied the Langmuir-Hinshelwood model assuming a first-order degradation mechanism [54]; only the linear part of the degradation curves were fitted, as indicated in the ISO 10678:2010 protocol. A value of $(1.25 \pm 0.06) \times 10^{-2}$ min^{-1} was found for the synthetized nanoparticles, while a value of $(1.41 \pm 0.07) \times 10^{-2}$ min^{-1} was found for the commercial ones (Table 2). In an effort to correlate these result with the morphological and structural properties of the powders, we can say that despite the higher surface area of the titania synthetized with the thyme extract than the one of commercial titania (see Table 1), the mixed anatase/rutile phase of the commercial material in comparison with the anatase phase of the titania synthetized with the thyme (see Figs. 2 and 3) makes the commercial powders slightly more performing than the powders synthetized by the authors, since the synergistic effects of the two different polymorphs [55,56].

Considering a possible future use of the titania powders here reported, the eventual toxicity of the nanoparticles was investigated. Fig. 7 shows the results of the toxicity tests of the TiO_2 nanoparticles synthetized with the thyme extract. In detail, Fig. 7 reports three microscopic images: a zebrafish embryo unexposed (a), a zebrafish embryo exposed to TiO_2 nanoparticles (b), a larva of zebrafish exposed to TiO_2 nanoparticles after hatching (c). The TiO_2 did not cause a significant percentage of coagulated eggs, which was ≤ 3% and it remained unchanged until the end of the tests. A sedimentation of the TiO_2 nanoparticles on the bottom of the well was observed, but anyway the embryos were mostly located on the bottom of the wells and then continually exposed to the nanoparticles. Before hatching, observations with the binocular

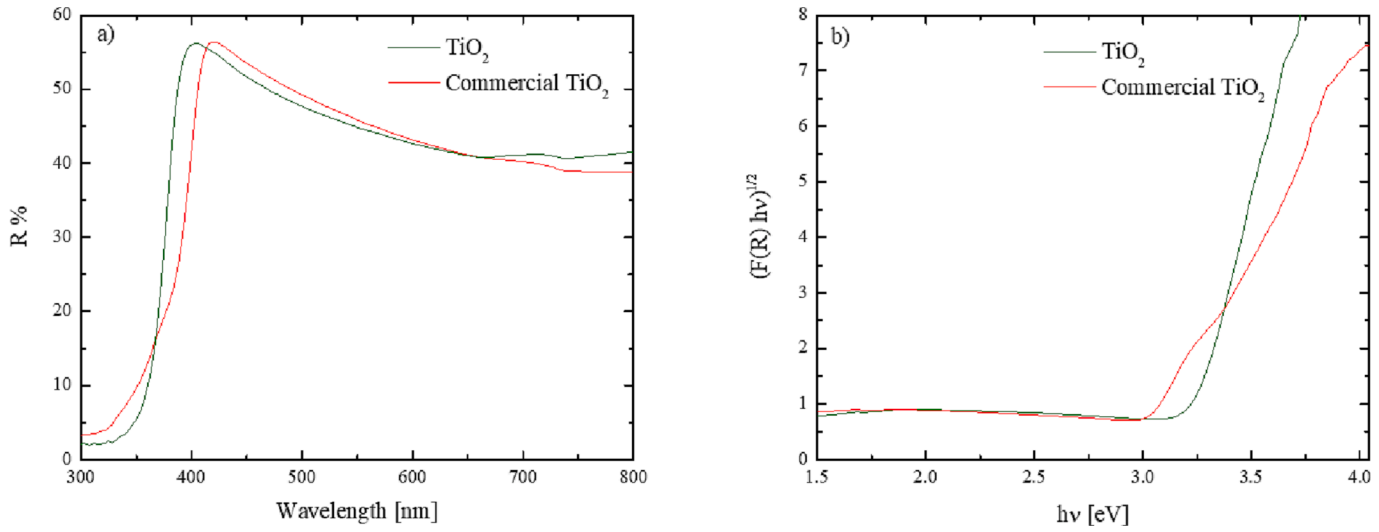

Fig. 5. (a) Diffuse reflectance spectra, and (b) Tauc plot of the Kubelka-Munk function of TiO_2 (green line) and commercial TiO_2 (red line) nanoparticles.

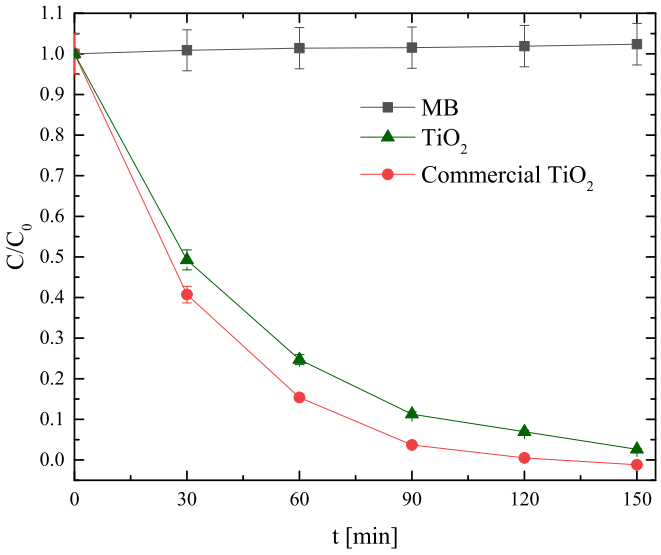

Fig. 6. MB photo-degradation under UV-light irradiation for three aqueous solutions: MB alone (squares), MB with TiO_2 synthetized with the thyme extract (triangles), MB with commercial TiO_2 (squares).

Table 2
Kinetic constant of the photocatalytic degradation of MB by TiO_2 synthetized with the thyme extract and by commercial TiO_2.

Catalyst	k (min^{-1})
TiO_2	$(1.25 \pm 0.06) \times 10^{-2}$
Commercial TiO_2	$(1.41 \pm 0.07) \times 10^{-2}$

microscope showed the deposition of the nanoparticles on the surface of the embryonic chorion (Fig. 7 (b)), that were not observed on the chorion of the unexposed embryo (Fig. 7 (a)). However, the constant permanence of the titania nanoparticles on the embryonic chorion did not interfere with the hatching of the embryos (Fig. 7 (c)). After 72 hpf almost all eggs were hatched. In addition, after hatching, the larvae appeared viable and with good shape of body despite being exposed to the nanoparticles.

Overall, toxicity can be excluded for this new TiO_2 nanoparticles because no embryo deaths or hatched larvae deaths were recorded. Despite, the embryonic chorion acts as a special structure surrounding the embryo to prevent the entry of pollutants [57]; the chorion pores have diameters between 300 nm and 1 μm, thus nano-pollutants with a certain size could pass through these to enter the embryo [58,59]. The synthetized TiO_2 showed a size of 10–15 nm (the reader can refer to the discussion of Fig. 4), for this reason the probability of its passage through the pores could be high; however, because of the agglomeration of the nanoparticles (see Fig. 1 (a) and 4 (a)) no alteration in embryonic development or body malformation were recorded in the embryos and hatched larvae.

In order to improve the photocatalytic efficiency of the synthetized titania, we decorated the TiO_2 powders with Ag nanoparticles (purchased from Merck), as reported in the Experimental section. SEM analysis of the commercial Ag (reported in Fig. S3) revealed nanoparticles with an irregular shapes and an average size lower than 100 nm, in agreement with what reported by Merck in the product specification. A more detailed investigation was performed thanks to TEM, and the results are shown in Fig. S4. HAADF-STEM analyses of commercial Ag nanoparticles (Fig. S4) highlighted a size distribution ranging from few nanometers to tens of nanometers. The silver was added because noble metals are notoriously efficient electron-scavenger thanks to the formation of a Schottky junction between the TiO_2 and the metal that improves the separation of the charge carriers, and hence the photocatalytic efficiency [3–5,8,11]. Several percentages of Ag nanoparticles (from 0.25 to 3% in weight, respect to the TiO_2) were investigated.

Table 3 reports the BET surface area (S_{BET}), the pore diameter (d_p), and the pore volume (V_p) of the different TiO_2 nanoparticles: pure TiO_2, TiO_2 + Ag 0.25%, TiO_2 + Ag 0.5%, TiO_2 + Ag 1%, TiO_2 + Ag 2%, TiO_2 + Ag 3%. Comparing the experimental results obtained for TiO_2 and TiO_2 + Ag 0.25%, the surface areas, neither the pore diameters nor the pore volumes changed; this is probably due to the low percentage of silver. Figure S5 (a) reports the N_2 adsorption–desorption curves, while Fig. S5 (b) shows the BJH pore size distributions of TiO_2 and TiO_2 + 0.25% Ag powders. Both the isotherms and the BJH distributions are very similar for the two different powders, further supporting the previous conclusion. On the other hand (Table 3), by increasing the silver percentage (from 0.5 to 3%) the surface area slightly decreases, probably due to an agglomeration process driven by the silver presence; while the pore diameters and the pore volumes are equal within the experimental error for the different silver percentage (from 0.5 to 3%).

FTIR spectra of the TiO_2 synthetized with the green method and enriched with the Ag nanoparticles are reported in Fig. S6. All the spectra showed similar features (for additional details the reader can refer to the discussion of Fig. S2). The presence of silver was not evidenced by the FTIR characterization [50].

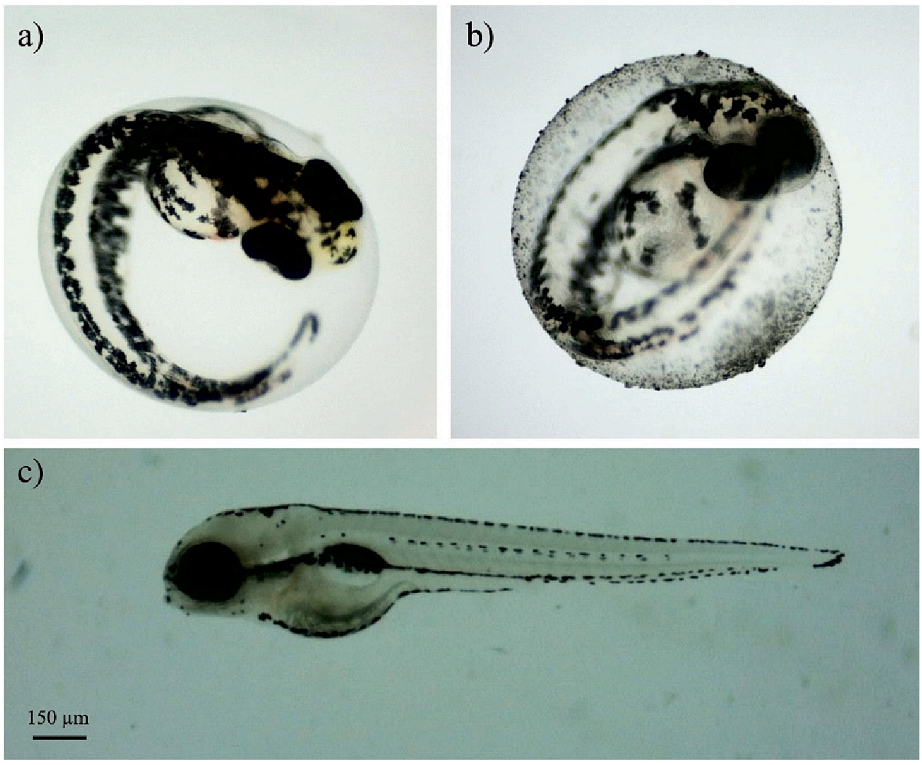

Fig. 7. (a) Zebrafish embryo unexposed to TiO_2 nanoparticles; (b) zebrafish embryo exposed to TiO_2 nanoparticles; (c) larva of zebrafish exposed to TiO_2 nanoparticles after hatching.

Table 3
BET surface area (S_{BET}), mean pore diameter (d_p), and pore volume (V_p) of TiO_2 synthetized with the thyme extract and decorated with several Ag percentage (from 0.25 to 3%).

Catalyst	S_{BET} ($m^2\ g^{-1}$)	d_p (nm)	V_p ($cm^3\ g^{-1}$)
TiO_2	92 ± 2	10.3 ± 0.5	0.28 ± 0.02
TiO_2 + Ag 0.25%	90 ± 2	11.0 ± 0.6	0.30 ± 0.02
TiO_2 + Ag 0.5%	88 ± 2	11.1 ± 0.6	0.31 ± 0.02
TiO_2 + Ag 1%	82 ± 2	11.5 ± 0.6	0.31 ± 0.02
TiO_2 + Ag 2%	78 ± 2	11.9 ± 0.6	0.30 ± 0.02
TiO_2 + Ag 3%	75 ± 2	11.6 ± 0.6	0.28 ± 0.02

XRD analyses were also conducted for the TiO_2/Ag powders in order to check their crystalline phase. Figure S7 shows the patterns of TiO_2 synthetized with the thyme extract and enriched with the silver nanoparticles. All the powders evidenced the peaks typical of the anatase phase. The absence of the Ag peaks maybe be due to the low concentration of the element and the small size of the silver nanoparticles. The crystal sizes, estimated by the Scherrer equation [52] were reported in Table S1. The dimensions are in the range between 85 and 94 nm for all the synthetized TiO_2 powders, regardless of the presence of silver. Thus, the Ag doping did not affect the crystallite sizes.

Raman investigations of the TiO_2 powders decorated with the silver nanoparticles, reported in Fig. S8, did not show any variation with respect to the spectra of the TiO_2 synthetized with the thyme extract. Indeed, all the spectra presented the typical peaks of the anatase phase.

A detailed TEM investigation of the TiO_2 + Ag 0.25% nanoparticles is reported in Fig. 8. HAADF S-TEM imaging (Fig. 8 (a)) showed aggregated TiO_2 nanoparticles having a mean size of about 10–15 nm, as observed in the case of the TiO_2 materials (see Fig. 4 (a)), but now decorated with Ag nanoparticles with a diameter of 1–2 nm. The Ag nanoparticles appear brighter compared to TiO_2 because in HAADF S-TEM imaging the signal intensity roughly varies with the square of the atomic number (*Z*-contrast). The inset of Fig. 8 (a) reports a magnified view of a single TiO_2 nanoparticle in which the (1 0 1) atomic planes with characteristic spacing of 0.35 nm are highlighted. The TiO_2 + Ag 0.25% nanoparticles were investigated in SI mode with EELS (Fig. 8 (b)) and EDS (Fig. 8 (c)) techniques. SI mode combines the spatial information acquired through the S-TEM detector with EELS and EDS data: for every spatial pixel acquired, one EELS spectrum and one EDS spectrum are simultaneously collected. This technique therefore provides spatially-resolved chemical information. To increase the signal-to-noise ratio, EELS and EDS data can be integrated over defined areas. SI technique was used to analyse the two areas enclosed by the boxes depicted in Fig. 8 (a). The red box was centred on a single Ag nanoparticle lying above a TiO_2 nanoparticle, while the light blue box enclosed a region of the same TiO_2 nanoparticle. Fig. 8 (b) reports the EELS spectra of TiO_2 obtained from the two different areas: the spectrum in red and in light blue are respectively related to the red and the light blue boxes. Similarly to Fig. 4 (b), EELS spectra both showed a split Ti L edge, starting at 455 eV, with the characteristic profile of anatase TiO_2, and a O K edge starting at 532 nm (inset of Fig. 8 (b)). No difference on the EELS fine structure can be noticed between the red and the light blue spectra, just a small change on the integral due to different specimen thickness. This is even confirmed by the inset of Fig. 8 (b) where the same EELS spectra is represented with a larger energy range just to include O K edge. This gave the evidence that the presence of the Ag nanoparticles has not a measurable effect since the distribution density of unoccupied states of the TiO_2 are practically unchanged when it is in contact with the Ag nanoparticles. This implies that the synthesis process did not induce a strong chemical bond between Ag and TiO_2, but weaker surface contact forces. Fig. 8 (c) shows two EDS spectra relative to the two boxes of Fig. 8 (a). Both spectra are characterized by signals coming from the TiO_2 nanoparticle (titanium Kα and Kβ peaks and oxygen Kα peak) and from the TEM grid (carbon Kα and copper Kα and Kβ peaks); the red EDS spectrum clearly shows the Ag L peak at 2.98 keV, originating from the silver nanoparticle enclosed in the red box (Fig. 8 (a)).

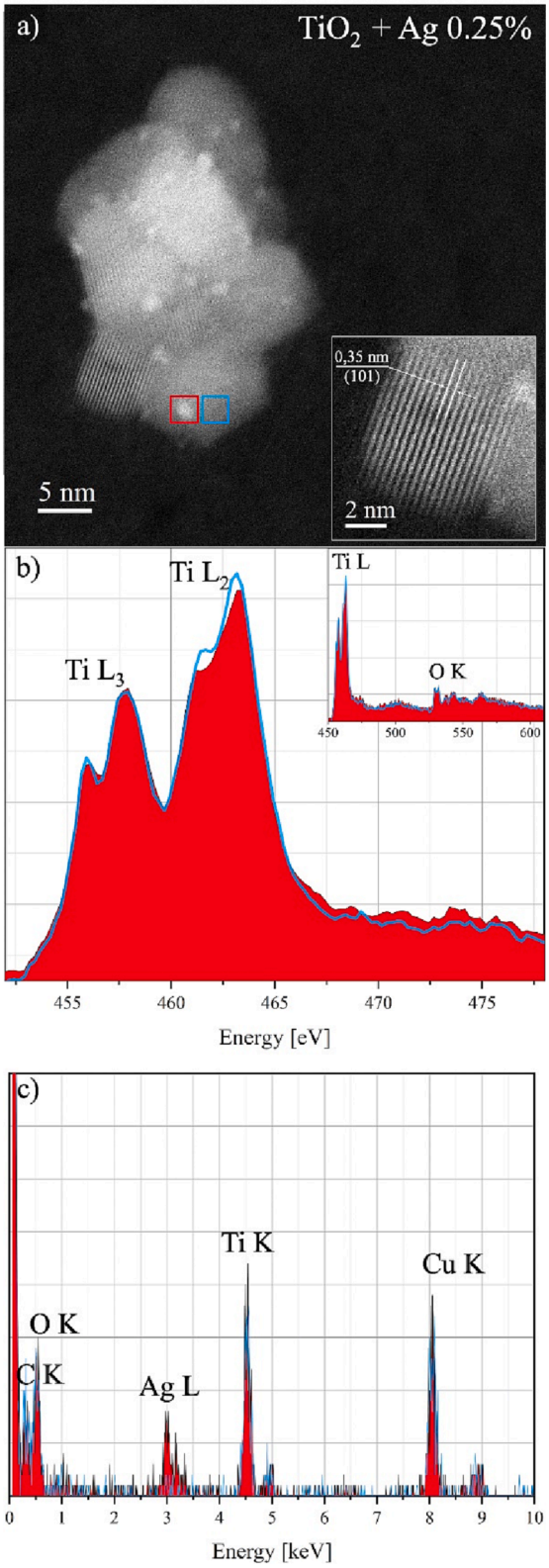

Fig. 8. (a) HAADF S-TEM micrograph of TiO_2 + Ag 0.25% nanoparticles, showing the TiO_2 nanoparticles decorated with the Ag nanoparticles. Inset shows a magnified view of a single TiO_2 nanoparticle, highlighting the (1 0 1) atomic planes; (b) EELS spectra of Ti L and O K edges of TiO_2 + Ag 0.25% nanoparticles. Red and light blue spectra respectively resulted from the red and light blue boxes depicted in Fig. 8 (a); (c) EDS spectra of TiO_2 + Ag 0.25% nanoparticles. Red and light blue spectra respectively resulted from the red and light blue boxes depicted in Fig. 8 (a). Red spectrum is characterized by the presence of Ag L peak at 2.98 keV.

From what observed with the TEM, we can deduce that during the preparation process of the TiO_2/Ag composites a size selection of the Ag nanoparticles takes place, indeed only the smallest ones (about 1–2 nm) were deposited on the surface of the TiO_2 (the reader can compare the Ag images reported in Fig. S4 and Fig. 8 (a). This is probably due to the higher surface-to-volume ratio of the smallest Ag nanoparticles, which make them more reactive and hence inclined to decorate the TiO_2.

HAADF-STEM analyses were also performed on TiO_2 + Ag 3%, and reported in Fig. S9. The image shows aggregated TiO_2 nanoparticles decorated with the Ag ones (3%).

The photocatalytic aptitude of the different composites (TiO_2 + Ag 0.25%, TiO_2 + Ag 0.5%, TiO_2 + Ag 1%, TiO_2 + Ag 2%, TiO_2 + Ag 3%) was firstly investigated by the MB dye discoloration. The control experiment under dark condition did not show any remarkable adsorption process. Fig. 9 reports the photocatalytic tests under UV light for the five composites compared to mere TiO_2 (we remind the reader that all the titania was synthetized with the thyme extract). A reference test was performed with an aqueous solution containing only the MB dye, and no response was obtained in this case (squares), as expected. On the other hand, the silver nanoparticles induced a clear enhancement of the photocatalytic behavior. In particular, the best result was obtained in the case of silver at 0.25%, which was able to degrade ~95% of the MB in 2 h (down triangles). The photo-degradation reaction rates of the MB contaminant by the different investigated samples were reported in Table 4. In particular, the kinetic constant was estimated at: $(2.81 \pm 0.14) \times 10^{-2}$ min^{-1} for the TiO_2 + Ag 0.25% samples, versus $(1.43 \pm 0.07) \times 10^{-2}$ min^{-1} for the TiO_2 reference samples. It is worth noting that by increasing the content of silver nanoparticles the photocatalytic efficiency decreases, even if always better than the one of mere TiO_2; this is the effect of a higher coverage of the titania surface by silver, that hinder the adsorption of the pollutant on the photocatalytic surface [11,60,61]. As a consequence, it is important to find the right quantity of metal nanoparticles in order to maximize their electron-scavenger effect. In this experiment, the best composite resulted the one with the lowest percentage of silver (only 0.25%).

The TiO_2 + Ag 0.25% samples were optically characterized, and a band-gap energy of 3.24 ± 0.05 eV was estimated. This value resulted equal within the experimental error to the value obtained for the mere TiO_2 powders, probably due to the low percentage of the added silver

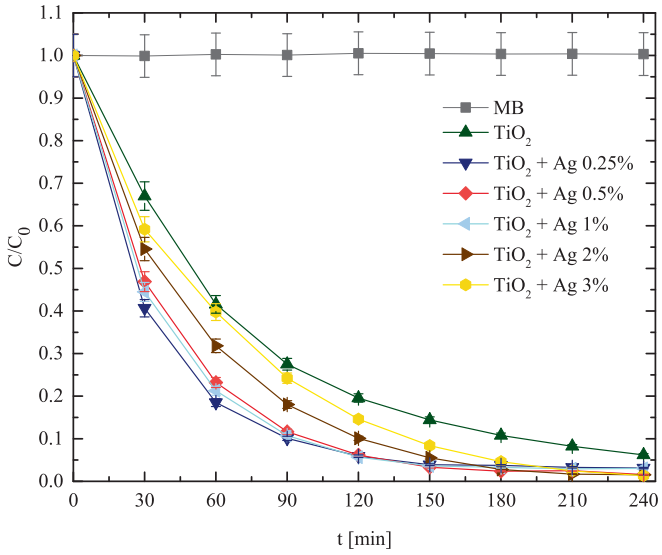

Fig. 9. MB photo-degradation under UV-light irradiation for seven samples: a solution of MB alone (squares), a solution of MB with TiO_2 (up triangles), with TiO_2 + Ag 0.25% (down triangles), with TiO_2 + Ag 0.5% (diamonds), with TiO_2 + Ag 1% (left triangles), with TiO_2 + Ag 2% (right triangles), or with TiO_2 + Ag 3% (hexagons) nanopowders.

Table 4
Kinetic constants of the photocatalytic degradation of MB by TiO_2 synthetized with the thyme extract and with several Ag percentages.

Catalyst	k (min^{-1})
TiO_2	$(1.43 \pm 0.07) \times 10^{-2}$
TiO_2 + Ag 0.25%	$(2.81 \pm 0.14) \times 10^{-2}$
TiO_2 + Ag 0.5%	$(2.43 \pm 0.12) \times 10^{-2}$
TiO_2 + Ag 1%	$(2.58 \pm 0.13) \times 10^{-2}$
TiO_2 + Ag 2%	$(1.91 \pm 0.10) \times 10^{-2}$
TiO_2 + Ag 3%	$(1.54 \pm 0.08) \times 10^{-2}$

nanoparticles.

The best composite (i.e., TiO_2 + Ag 0.25%) was also tested for the degradation of diclofenac in comparison to mere TiO_2. The results reported in Fig. 10 indicated, again, the best performance of the samples decorated with the Ag nanoparticles (down triangles). Table 5 reports the photo-degradation reaction rates of diclofenac by the investigated samples. A worse efficiency was observed with respect to the MB dye (the reader can easily compare Fig. 9 and Fig. 10). This can be due to a higher quantity of diclofenac used (5.5×10^{-5} M) in the aqueous solution with respect to MB (1.5×10^{-5} M) necessary to maximize the absorbance peak, but it can be also due to the recalcitrant nature of the diclofenac [62].

A final photocatalytic test was performed with the SDS contamination. SDS is one of the main pollutant in greywater, being an anionic surfactant found in most personal hygiene products. Fig. 11 shows the experimental results obtained after a UV-light irradiation for 4 h for three samples typologies: an aqueous solution of SDS, an aqueous solution of SDS with TiO_2 nanopowders, and an aqueous solution of SDS containing TiO_2 + Ag 0.25% nanopowders. The TiO_2 + Ag 0.25% nanopowders were notably effective in degrading SDS: after 4 h almost all the SDS was degraded, indicating again the beneficial effect of the silver nanoparticles as effective electron-scavenger.

Table 5
Kinetic constants of the photocatalytic degradation of diclofenac by TiO_2 and TiO_2 + Ag 0.25%.

Catalyst	k (min^{-1})
TiO_2	$(0.52 \pm 0.03) \times 10^{-2}$
TiO_2 + Ag 0.25%	$(0.89 \pm 0.04) \times 10^{-2}$

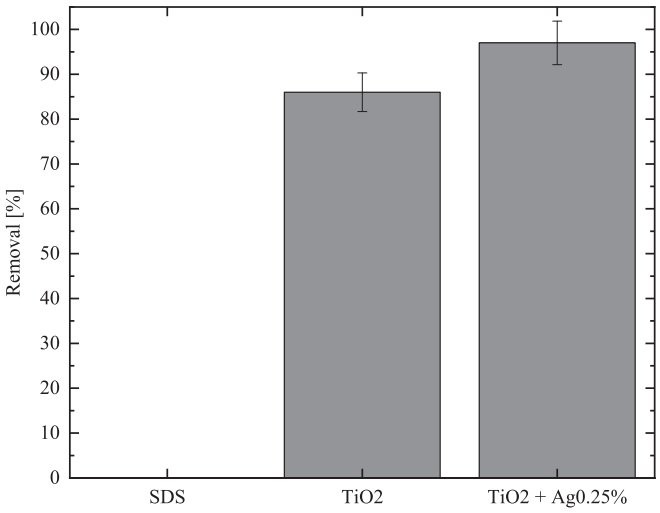

Fig. 11. SDS photo-degradation after 4 h of UV-light irradiation for three samples: a solution of SDS alone (squares), a solution of SDS with TiO_2, or with TiO_2 + Ag 0.25% nanopowders.

The toxicity tests were repeated in the case of the TiO_2 + Ag 0.25% nanoparticles, which arose the best photocatalytic composite among the tested compositions. The results are reported in Fig. 12. Even in embryos

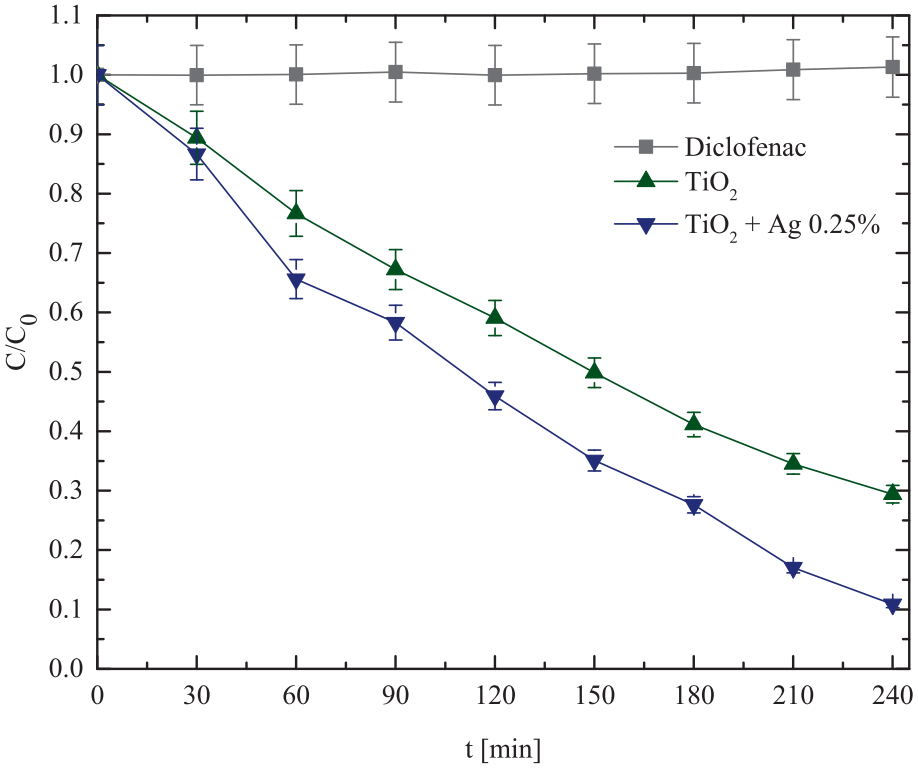

Fig. 10. Diclofenac photo-degradation under UV-light irradiation for three samples: a solution of diclofenac alone (squares), a solution of diclofenac with TiO_2 (up triangles), a solution of diclofenac with TiO_2 + Ag 0.25% (down triangles) nanopowders.

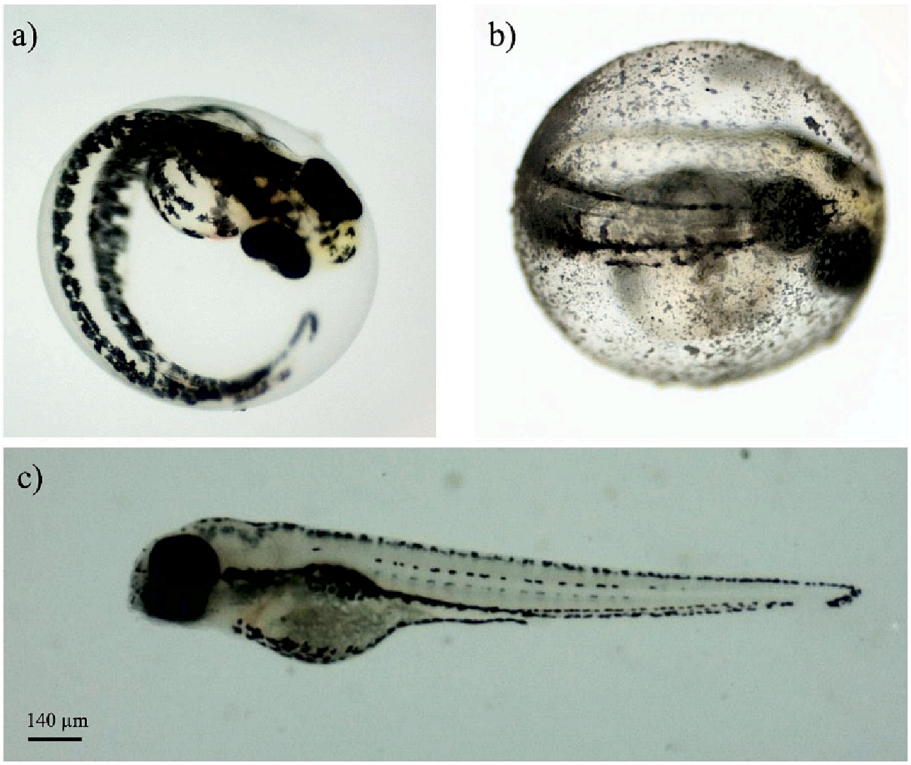

Fig. 12. (a) Zebrafish embryo unexposed to TiO_2 + Ag 0.25% nanoparticles; (b) zebrafish embryo exposed to TiO_2 + Ag 0.25% nanoparticles; (c) larva of zebrafish exposed to TiO_2 + Ag 0.25% nanoparticles after hatching.

exposed to the TiO_2 + Ag 0.25% nanoparticles no egg coagulation and interference in hatching were observed. The nanoparticles adhered to the embryonic chorion as evidenced in the micrograph in Fig. 12 (b). After 72 hpf almost all eggs were hatched. Nanoparticles diffusion may be toxic to embryo development during the period of organogenesis [58]. Several studies have shown that single Ag nanoparticles (5–46 nm in size) are transported into embryos through chorion pore canals and caused effects on embryonic development that include fin fold abnormality, tail and spinal cord flexure and truncation, cardiac malformation, yolk sac edema, head edema, and eye abnormality [63–66]. The lack of similar anomalies highlighted the no toxicity of the investigated TiO_2 + Ag 0.25% nanoparticles.

4. Conclusions

In conclusion, we presented an original, simple, and green method to synthesize TiO_2 nanoparticles. The preparation of the powders was performed by Thymus vulgaris leaf extract. The green titania nanoparticles revealed a mean size of ~10–15 nm and a crystallographic phase of the anatase. They also showed a remarkable photocatalytic aptitude compared to the one of commercial TiO_2. To improve the photocatalytic efficiency of the green TiO_2 powders, they were decorated with commercial Ag nanoparticles (<100 nm particle size). Several silver percentages (in weight compared to the titanium dioxide) were investigated (from 0.25 to 3%). During the preparation process of the TiO_2/Ag composites a size selection of the Ag nanoparticles took place, indeed only the smallest ones (about 1–2 nm) were deposited on the surface of the TiO_2. The TiO_2/Ag composite with the lowest silver percentage (0.25%) resulted the best photocatalyst, able to efficiently degrade several organic contaminants. Thus, the best result was obtained with the lowest price. The safety of the nanopowders was demonstrated by the zebrafish embryo toxicity tests. This work opens the route to the use of the green titania as photocatalyst for an efficient and environmental-friendly wastewater remediation.

CRediT authorship contribution statement

Maria Cantarella: Visualization, Investigation, Formal analysis, Data curation. **Marco Mangano:** Visualization, Investigation. **Massimo Zimbone:** Visualization, Investigation. **Gianfranco Sfuncia:** Visualization, Investigation. **Giuseppe Nicotra:** Visualization, Investigation. **Elena Maria Scalisi:** Investigation, Visualization. **Maria Violetta Brundo:** Visualization, Investigation, Formal analysis, Data curation. **Anna Lucia Pellegrino:** Investigation, Visualization. **Federico Giuffrida:** Investigation. **Vittorio Privitera:** Funding acquisition. **Giuliana Impellizzeri:** Writing – original draft, Supervision, Funding acquisition, Conceptualization.

Declaration of Competing Interest

The authors declare that they have no known competing financial interests or personal relationships that could have appeared to influence the work reported in this paper.

Data availability

No data was used for the research described in the article.

Acknowledgement

The authors wish to thank Francesco La Via (CNR-IMM) for the access to the Raman laboratory, Giuseppe Pantè (CNR-IMM) and Salvatore Pannitteri (CNR-IMM) for technical assistance. This work has been partially funded by the project PO-FESR Sicilia MiaCasa (CUP: G68I18000650007). The TEM analyses were performed at BeyondNano CNR-IMM laboratory, which is supported by the European Commission's Horizon 2020 Research and Innovation program under the Grant Agreement no. 823717. A. L. P. thanks the Bionanotech Research and Innovation Tower (BRIT) laboratory of University of Catania (Grant no.

PONa3_00136 financed by the Italian Ministry for Education, University and Research, MIUR) for the diffractometer facility and the Ministero dell'Università e della Ricerca within the PON "Ricerca e Innovazione" 2014-2020 Azioni IV.4 program.

Appendix A. Supplementary data

Supplementary data to this article can be found online at https://doi.org/10.1016/j.jphotochem.2023.114838.

References

[1] A. Fujishima, K. Honda, Electrochemical photolysis of water at a semiconductor electrode, Nature 238 (1972) 37–38, https://doi.org/10.1038/238037a0.

[2] A. Fujishima, T.N. Rao, D.A. Tryk, Titanium dioxide photocatalysis, J. Photochem. Photobiol. C: Photochem. Rev. 1 (2000) 1–21, https://doi.org/10.1016/S1389-5567(00)00002-2.

[3] T.L. Thompson, J.T. Yates Jr., Surface science studies of the photoactivation of TiO_2-New photochemical processes, Chem. Rev. 106 (2006) 4428–4453, https://doi.org/10.1021/cr050172k.

[4] X. Chen, S.S. Mao, Titanium dioxide nanomaterials: Synthesis, properties, modifications, and applications, Chem. Rev. 107 (2007) 2891–2959, https://doi.org/10.1021/cr0500535.

[5] U.I. Gaya, A.H. Abdullah, Heterogeneous photocatalytic degradation of organic contaminants over titanium dioxide: A review of fundamentals, progress and problems, J. Photochem. Photobiol. C 9 (2008) 1–12, https://doi.org/10.1016/j.jphotochemrev.2007.12.003.

[6] Z. Zhao, J. Tian, Y. Sang, A. Cabot, H. Liu, Structure, synthesis, and applications of TiO_2 nanobelts, Adv. Mater. 27 (2015) 2557–2582, https://doi.org/10.1002/adma.201405589.

[7] R. Katal, S. Masudy-Panah, M. Tanhaei, M.H.D.A. Farahani, H. Jiangyong, A review on the synthesis of the various type of anatase TiO_2 facets and their applications in photocatalysis, Chem. Eng. J. 384 (123384) (2020) 1–26, https://doi.org/10.1016/j.cej.2019.123384.

[8] W. Zhang, Y. Tian, H. He, L. Xu, W. Li, D. Zhao, Recent advances in the synthesis of hierarchically mesoporous TiO_2 materials for energy and environmental applications, Natl. Sci. Rev. 7 (2020) 1702–1725, https://doi.org/10.1093/nsr/nwaa021.

[9] S.N. Frank, A.J. Bard, Heterogeneous photocatalytic oxidation of cyanide and sulfite in aqueous solutions at semiconductor powders, J. Phys. Chem. 81 (1977) 1484–1488, https://doi.org/10.1021/j100530a011.

[10] G. Impellizzeri, V. Scuderi, L. Romano, P.M. Sberna, E. Arcadipane, R. Sanz, M. Scuderi, G. Nicotra, M. Bayle, R. Carles, F. Simone, V. Privitera, Fe ion-implanted TiO_2 thin film for efficient visible-light photocatalysis, J. Appl. Phys. 116 (173507) (2014) 1–8, https://doi.org/10.1063/1.4901208.

[11] V. Scuderi, G. Impellizzeri, L. Romano, M. Scuderi, M.V. Brundo, K. Bergum, M. Zimbone, R. Sanz, M.A. Buccheri, F. Simone, G. Nicotra, B.G. Svensson, M. G. Grimaldi, V. Privitera, An enhanced photocatalytic response of nanometric TiO_2 wrapping of Au nanoparticles for eco-friendly water applications, Nanoscale 6 (2014) 11189–11195, https://doi.org/10.1039/c4nr02820a.

[12] V. Scuderi, G. Impellizzeri, L. Romano, M. Scuderi, G. Nicotra, K. Bergum, A. Irrera, B.G. Svensson, V. Privitera, TiO_2 coated nanostructures for dye photo-degradation in water, Nanoscale Res. Lett. 9 (458) (2014) 1–7, https://doi.org/10.1186/1556-276X-9-458.

[13] G. Impellizzeri, V. Scuderi, L. Romano, E. Napolitani, R. Sanz, R. Carles, V. Privitera, C ion-implanted TiO_2 thin film for photocatalytic applications, J. Appl. Phys. 117 (105308) (2015) 1–6, https://doi.org/10.1063/1.4915111.

[14] M. Zimbone, M.A. Buccheri, G. Cacciato, R. Sanz, G. Rappazzo, S. Boninelli, R. Reitano, L. Romano, V. Privitera, M.G. Grimaldi, Photocatalytical and antibacterial activity of TiO_2 nanoparticles obtained by laser ablation in water, Appl. Catal. B 165 (2015) 487–494, https://doi.org/10.1016/j.apcatb.2014.10.031.

[15] R. Sanz, L. Romano, M. Zimbone, M.A. Buccheri, V. Scuderi, G. Impellizzeri, M. Scuderi, G. Nicotra, J. Jensen, V. Privitera, UV-black rutile TiO_2: An antireflective photocatalytic nanostructure, J. Appl. Phys. 117 (074903) (2015) 1–8, https://doi.org/10.1063/1.4913222.

[16] V. Scuderi, M.A. Buccheri, G. Impellizzeri, A. Di Mauro, G. Rappazzo, K. Bergum, B. G. Svensson, V. Privitera, Photocatalytic and antibacterial properties of titanium dioxide flat films, Mater. Sci. Semicond. Process. 42 (2016) 32–35, https://doi.org/10.1016/j.mssp.2015.09.005.

[17] V. Scuderi, G. Impellizzeri, M. Zimbone, R. Sanz, A. Di Mauro, M.A. Buccheri, M. Miritello, A. Terrasi, G. Rappazzo, G. Nicotra, V. Privitera, Rapid synthesis of photoactive hydrogenated TiO_2 nanoplumes, Appl. Catal. B 183 (2016) 328–334, https://doi.org/10.1016/j.apcatb.2015.10.055.

[18] A. Convertino, L. Maiolo, V. Scuderi, A. Di Mauro, M. Scuderi, G. Nicotra, G. Impellizzeri, G. Fortunato, V. Privitera, A forest of SiO_2 nanowires covered by a TiO_2 thin film for an efficient photocatalytic water treatment, RSC Adv. 6 (2016) 91121–91126, https://doi.org/10.1039/c6ra15986a.

[19] M. Cantarella, R. Sanz, M.A. Buccheri, F. Ruffino, G. Rappazzo, S. Scalese, G. Impellizzeri, L. Romano, V. Privitera, Immobilization of nanomaterials in PMMA composites for photocatalytic removal of dyes, phenols and bacteria from water, J. Photochem. Photobiol. A 321 (2016) 1–11, https://doi.org/10.1016/j.jphotochem.2016.01.020.

[20] V. Scuderi, G. Amiard, R. Sanz, S. Boninelli, G. Impellizzeri, V. Privitera, TiO_2 coated CuO nanowire array: Ultrathin p–n heterojunction to modulate cationic/anionic dye photo-degradation in water, Appl. Surf. Sci. 416 (2017) 885–890, https://doi.org/10.1016/j.apsusc.2017.04.229.

[21] M. Cantarella, G. Impellizzeri, V. Privitera, Functional nanomaterials for water purification, Riv. del Nuovo Cim. 40 (2017) 595–632, https://doi.org/10.1393/ncr/i2017-10142-8.

[22] M. Zimbone, M. Cantarella, G. Impellizzeri, S. Battiato, L. Calcagno, Synthesis and photochemical properties of monolithic TiO_2 nanowires diode, Molecules 26 (3636) (2021) 1–10, https://doi.org/10.3390/molecules26123636.

[23] M. Zimbone, M. Cantarella, G. Sfuncia, G. Nicotra, V. Privitera, E. Napolitani, G. Impellizzeri, Low-temperature atomic layer deposition of TiO_2 activated by laser annealing: Applications in photocatalysis, Appl. Surf. Sc. 596 (153641) (2022) 1–9, https://doi.org/10.1016/j.apsusc.2022.153641.

[24] H.K. Bayabil, F.T. Teshome, Y.C. Li, Emerging contaminants in soil and water, Front. Environ. Sci. 10 (2022), 873499, https://doi.org/10.3389/fenvs.2022.873499.

[25] J.G. Mahy, S.D. Lambert, G.-L.-M. Léonard, A. Zubiaur, P.-Y. Olu, A. Mahmoud, F. Boschini, B. Heinrichs, Towards a large scale aqueous sol-gel synthesis of doped TiO_2: Study of various metallic dopings for the photocatalytic degradation of p nitrophenol, J. Photochem. Photobiol. A 329 (2016) 189–202, https://doi.org/10.1016/j.jphotochem.2016.06.029.

[26] L. Andronic, D. Ghica, M. Stefan, C.G. Mihalcea, A.-M. Vlaicu, S. Karazhanov, Visible-light-active black TiO_2 nanoparticles with efficient photocatalytic performance for degradation of pharmaceuticals, Nanomaterials 12 (2563) (2022) 1–17, https://doi.org/10.3390/nano12152563.

[27] S. Chin, E. Park, M. Kim, J. Jurng, Photocatalytic degradation of methylene blue with TiO_2 nanoparticles prepared by a thermal decomposition process, Powder Technol. 201 (2010) 171–176, https://doi.org/10.1016/j.powtec.2010.03.034.

[28] S. Ko, C.K. Banerjee, J. Sankar, Photochemical synthesis and photocatalytic activity in simulated solar light of nanosized Ag doped TiO_2 nanoparticle composite, Compos. B Eng. 42 (2011) 579–583, https://doi.org/10.1016/j.compositesb.2010.09.007.

[29] A. Guimarães de Oliveira, J.P. Nascimento, H.F. Gorgulho, P.B. Martelli, C. A. Furtado, J.L. Figueiredo, Electrochemical synthesis of TiO_2/Graphene oxide composite films for photocatalytic applications, J. Alloys Compd. 654 (2016) 514–522, https://doi.org/10.1016/j.jallcom.2015.09.110.

[30] R. Cao, J. Gao, H. Tao, One-step hydrothermal synthesis of multiphase nano TiO_2, Mater. Lett. 317 (132121) (2022) 1–4, https://doi.org/10.1016/j.matlet.2022.132121.

[31] M. Scarisoreanu, I. Morjan, C.-T. Fleaca, I.P. Morjan, A.-M. Niculescu, E. Dutu, A. Badoi, R. Birjega, C. Luculescu, E. Vasile, V. Danciu, G. Filot, Synthesis and optical properties of TiO_2-based magnetic nanocomposites, Appl. Surf. Sci. 336 (2015) 335–342, https://doi.org/10.1016/j.apsusc.2014.12.125.

[32] Y. Wang, Y. He, Q. Lai, M. Fan, Review of the progress in preparing nano TiO_2: An important environmental engineering material, J. Environ. Sci. 26 (2014) 2139–2177, https://doi.org/10.1016/j.jes.2014.09.023.

[33] S. Jadoun, R. Arif, N.K. Jangid, R.K. Meena, Green synthesis of nanoparticles using plant extracts: A review, Environ. Chem. Lett. 19 (2021) 355–374, https://doi.org/10.1007/s10311-020-01074-x.

[34] A. Joseph, A. Vijayanandan, Photocatalysts synthesized via plant mediated extracts for degradation of organic compounds: A review of formation mechanisms and application in wastewater treatment, Sustain. Chem. Pharm. 22 (100453) (2021) 1–16, https://doi.org/10.1016/j.scp.2021.100453.

[35] S.P. Goutama, G. Saxena, V. Singh, A.K. Yadav, R.N. Bharagava, K.B. Thapa, Green synthesis of TiO_2 nanoparticles using leaf extract of *Jatropha curcas* L. for photocatalytic degradation of tannery wastewater, Chem. Eng. J. 336 (2018) 386–396, https://doi.org/10.1016/j.cej.2017.12.029.

[36] N. Arabi, A. Kianvash, A. Hajalilou, E. Aboozari-Lotf, V. Abbasi-Chianeh, A facile and green synthetic approach toward fabrication of Alcea- and Thyme-stabilized TiO_2 nanoparticles for photocatalytic applications, Arab. J. Chem. 13 (2020) 2132–2141, https://doi.org/10.1016/j.arabjc.2018.03.014.

[37] H. Kaur, S. Kaur, J. Singh, M. Rawat, Eco-friendly approach: Synthesis of novel green TiO_2 nanoparticles for degradation of reactive green 19 dye and replacement of chemical synthesized TiO_2, J. Clust. Sci. 32 (2021) 1191–1204, https://doi.org/10.1007/s10876-020-01881-w.

[38] V. Prasanth Reddy, R.V. Kandisa, P.V. Varsha, S. Satyam, Review on Thymus vulgaris traditional uses and pharmacological properties, Int. J. Med. Aromat. Plants. 3 (4) (2014) 1–3, https://doi.org/10.4172/2167-0412.1000167.

[39] M. Kazemi, Phytochemical composition of Thymus vulgaris L, essential Oil, J. Essent. Oil Bear Pl. 18 (3) (2015) 751–753, https://doi.org/10.1080/0972060X.2014.985733.

[40] J.F. Vouillamoz, B. Christ, Thymus vulgaris L.: Thyme, in: J. Novak, W.D. Blüthner (Eds.), Medicinal, Aromatic and Stimulant Plants. Handbook of Plant Breeding, vol 12, Springer, Cham, 2020, https://doi.org/10.1007/978-3-030-38792-1_18.

[41] P. Makuła, M. Pacia, W. Macyk, How To correctly determine the band gap energy of modified semiconductor photocatalysts based on UV–Vis spectra, J. Phys. Chem. Lett. 9 (23) (2018) 6814–6817, https://doi.org/10.1021/acs.jpclett.8b02892.

[42] R. Wang, K. Hashimoto, A. Fujishima, M. Chikuni, E. Kojima, A. Kitamura, M. Shimohigoshi, T. Watanabe, Light-induced amphiphilic surfaces, Nature 388 (1997) 431–432, https://doi.org/10.1038/41233.

[43] A. D. McNaught, A. Wilkinson, in Compendium of Chemical Terminology, Blackwell Scientific Publications, Oxford, 2nd edn., 1997; "the Gold Book".

[44] C. Nüsselin-Volhard, R. Dahm, in Zebrafish a Practical Approach, Oxford, University Press, New York, USA, 2000.
[45] R. Pecoraro, F. Marino, A. Salvaggio, F. Capparucci, G. Di Caro, C. Iaria, A. Salvo, A. Rotondo, D. Tibullo, G. Guerriero, E.M. Scalisi, M. Zimbone, G. Impellizzeri, M. V. Brundo, Evaluation of chronic nanosilver toxicity to adult zebrafish, Front. Physiol. 8 (1011) (2017) 1–9, https://doi.org/10.3389/fphys.2017.01011.
[46] R. Pecoraro, A. Salvaggio, F. Marino, G. Di Caro, F. Capparucci, B.M. Lombardo, G. Messina, E.M. Scalisi, M. Tummino, F. Loreto, G. D'Amante, R. Avola, D. Tibullo, M.V. Brundo, Metallic nano-composite toxicity evaluation by zebrafish embryo toxicity test with identification of specific exposure biomarkers, Curr. Protoc. Toxicol. 74 (1) (2017) 1–14, https://doi.org/10.1002/cptx.34.
[47] H. Çolak, E. Karaköse, Structural, electrical and optical properties of green synthesized ZnO nanoparticles using aqueous extract of thyme (*Thymus vulgaris*), J. Mater. Sci.: Mater. Electron. 28 (2017) 12184–12190, https://doi.org/10.1007/s10854-017-7033-0.
[48] M. Zare, K. Namratha, M.S. Thakur, K. Byrappa, Biocompatibility assessment and photocatalytic activity of bio-hydrothermal synthesis of ZnO nanoparticles by Thymus vulgaris leaf extract, Mater. Res. Bull. 109 (2019) 49–59, https://doi.org/10.1016/j.materresbull.2018.09.025.
[49] J. Yu, G. Wang, B. Cheng, M. Zhou, Effects of hydrothermal temperature and time on the photocatalytic activity and microstructures of bimodal mesoporous TiO_2 powders, Appl. Catal. B. Environ. 69 (2007) 171–180, https://doi.org/10.1016/j.apcatb.2006.06.022.
[50] A. Rostami-Vartooni, M. Nasrollahzadeh, M. Salavati-Niasari, M. Atarod, Photocatalytic degradation of azo dyes by titanium dioxide supported silver nanoparticles prepared by a green method using *Carpobrotus acinaciformis* extract, J. Alloys Compd. 689 (2016) 15–20, https://doi.org/10.1016/j.jallcom.2016.07.253.
[51] D.A.H. Hanaor, C.C. Sorrell, Review of the anatase to rutile phase transformation, J. Mater. Sci. 46 (4) (2011) 855–874, https://doi.org/10.1007/s10853-010-5113-0.
[52] A. Patterson, The Scherrer formula for X-ray particle size determination, Phys. Rev. 56 (10) (1939) 978–982, https://doi.org/10.1103/PhysRev.56.978.
[53] O. Frank, M. Zukalova, B. Laskova, J. Kurti, J. Koltai, L. Kavan, Raman spectra of titanium dioxide (anatase, rutile) with identified oxygen isotopes (16, 17, 18), Phys. Chem. Chem. Phys. 14 (2012) 14567–14572, https://doi.org/10.1039/C2CP42763J.
[54] M.N. Chong, B. Jin, C.W.K. Chow, C. Saint, Recent developments in photocatalytic water treatment technology: a review, Water Res. 44 (2010) 2997–3027, https://doi.org/10.1016/j.watres.2010.02.039.
[55] B. Ohtani, O.O. Prieto-Mahaney, D. Li, R. Abe, What is Degussa (Evonik) P25? Crystalline composition analysis, reconstruction from isolated pure particles and photocatalytic activity test, J. Photochem. Photobiol. A 216 (2010) 179–182, https://doi.org/10.1016/j.jphotochem.2010.07.024.
[56] T. Luttrell, S. Halpegamage, J. Tao, A. Kramer, E. Sutter, M. Batzill, Why is anatase a better photocatalyst than rutile? - Model studies on epitaxial TiO_2 films, Sci. Rep. 4 (4043) (2014) 1–8, https://doi.org/10.1038/srep04043.
[57] L.A. Kristofco, S.P. Haddad, C.K. Chambliss, B.W. Brooks, Differential uptake of and sensitivity to diphenhydramine in embryonic and larval zebrafish, Environ. Toxicol. Chem. 37 (4) (2018) 1175–1181, https://doi.org/10.1002/etc.4068.
[58] J. Cheng, E. Flahaut, S.H. Cheng, Effect of carbon nanotubes on developing zebrafish (Danio rerio) embryos, Environ. Toxicol. Chem. 26 (4) (2007) 708–716, https://doi.org/10.1897/06-272R.1.
[59] K. Fent, C.J. Weisbrod, A. Wirth-Heller, U. Pieles, Assessment of uptake and toxicity of fluorescent silica nanoparticles in zebrafish (*Danio rerio*) early lifestages, Aquat. Toxicol. 100 (2010) 218–228, https://doi.org/10.1016/j.aquatox.2010.02.019.
[60] I.M. Arabatzis, T. Stergiopoulos, D. Andreeva, S. Kitova, S.G. Neophytides, P. Falaras, Characterization and photocatalytic activity of Au/TiO_2 thin films for azo-dye degradation, J. Catal. 220 (2003) 127–135, https://doi.org/10.1016/S0021-9517(03)00241-0.
[61] L. Armelao, D. Barreca, G. Bottaro, A. Gasparotto, C. Maccato, C. Maragno, E. Tondello, U.L. Stangar, M. Bergant, D. Mahne, Photocatalytic and antibacterial activity of TiO_2 and Au/TiO_2 nanosystems, Nanotechnology 18 (375709) (2007) 1–7, https://doi.org/10.1088/0957-4484/18/37/375709.
[62] R. Banaschik, H. Jablonowski, P.J. Bednarski, J.F. Kolb, Degradation and intermediates of diclofenac as instructive examplefor decomposition of recalcitrant pharmaceuticals by hydroxylradicals generated with pulsed corona plasma in water, J. Hazard. Mater. 342 (2018) 651–660, https://doi.org/10.1016/j.jhazmat.2017.08.058.
[63] K.J. Lee, L.M. Browning, P.D. Nallathamby, C.J. Osgood, X.-H.-N. Xu, In vivo imaging of transport and biocompatibility of single silver nanoparticles in early development of zebrafish embryos, ACS Nano 1 (2007) 133–143, https://doi.org/10.1021/nn700048y.
[64] K.J. Lee, L.M. Browning, P.D. Nallathamby, C.J. Osgood, X.-H. Xu, Silver nanoparticles induce developmental stage-specific embryonic phenotypes in zebrafish, Nanoscale 5 (23) (2013) 11625, https://doi.org/10.1039/C3NR03210H.
[65] L.M. Browning, K.J. Lee, P.D. Nallathamby, X.-H.-N. Xu, Silver nanoparticles incite size and dose-dependent developmental phenotypes and nanotoxicity in zebrafish embryos, Chem. Res. Toxicol. 26 (2013) 1503–1513, https://doi.org/10.1021/tx400228p.
[66] M.S. Johnson, P. Songkiatisak, P.K. Cherukuri, X.-H. Xu, Toxic Effects of silver ions on early developing zebrafish embryos distinguished from silver nanoparticles, ACS Omega 7 (44) (2022) 40446–40455, https://doi.org/10.1021/acsomega.2c05504.